Nanoscale

PAPER

View Article Online
View Journal | View Issue

Check for updates

Cite this: *Nanoscale*, 2018, **10**, 4727

High-performance optical projection controllable ZnO nanorod arrays for microweighing sensors†

Hongbo Wang, [a] Shulan Jiang,[a] Lei Zhang,[b] Bingjun Yu,[a] Duoli Chen,[a] Weiqing Yang*[b] and Linmao Qian *[a]

Received 6th December 2017,
Accepted 8th February 2018

DOI: 10.1039/c7nr09076e

rsc.li/nanoscale

Optical microweighing sensors are an essential component of micro-force measurements in physical, chemical, and biological detection fields, although, their limited detection range (less than 15°) severely hinders their wide application. Such a limitation is mainly attributed to the essential restrictions of traditional light reflection and optical waveguide modes. Here, we report a high-performance optical microweighing sensor based on the synergistic effects of both a new optical projection mode and a ZnO nanorod array sensor. Ascribed to the unique configuration design of this sensing method, this optical microweighing sensor has a wide detection range (more than 80°) and a high sensitivity of 90 nA deg^{-1}, which is much larger than that of conventional microcantilever-based optical microweighing sensors. Furthermore, the location of the UV light source can be adjusted within a few millimeters, meaning that the microweighing sensor does not need repetitive optical calibration. More importantly, for low height and small incident angles of the UV light source, we can obtain highly sensitive microweighing properties on account of the highly sensitive ZnO nanorod array-based UV sensor. Therefore, this kind of large detection range, non-contact, and non-destructive microweighing sensor has potential applications in air quality monitoring and chemical and biological detection.

Introduction

A micro-force sensor is a crucial component in micro-component measuring, which is a pivotal part of many fields, such as biochemistry applications, materials science, micromanipulation, industrial automation, *et al.*[1] Usually, micro-force sensors can be generally classified into capacitive, piezoresistive, inductive, piezoelectric, magnetic, and optical types. Amongst these, optical type sensors are one of the most promising technologies due to their electromagnetic immunity and non-contact, high accuracy, and high resolution properties.[2] However, the complex configuration, high cost, and poor integration and compatibility with the microelectronics industry limit their large-scale commercial application. Hence, it is highly desired to fabricate an optical micro-force sensor with simultaneously simple structure, low cost, and the ability to integrate on a large scale.

Recently, microcantilever-based optical force sensors have been proven to be a robust way to convert various forces into an electric signal, due to a coupling effect between the microcantilever deflection and photovoltaic conversion.[3–5] On account of such outstanding properties as high performance, simple structure, low cost, and wide application potential, this type of sensor has been continuously developed based on optical lever,[6] photo-thermal,[7,8] and optical waveguide[9–12] modes. However, these modes depend heavily on the location of the laser spot and accurate optical calibration.[13–15] In particular, their deflecting detection ranges are often within 5–15° due to the limitation of the position-sensitive detector.[5,16] For instance, atomic force microscopy (AFM) is the typical application of optical lever mode, and its effective detection range is usually less than 15°.[13] Furthermore, Singamaneni *et al.* summarized photo-thermal sensors and indicated that their deflection ranges are usually within 5°.[5] Recently, Siwak *et al.* reported a resonant cantilever sensor based on an optical waveguide mode for micro-mass detection, whose effective detection range is also less than 5°.[9] Clearly, in the above mentioned optical micro-force sensors, one of the most common flaws is that they cannot detect micro-force once the deflection of the microcantilever is more than 15°. Due to such limitations, microcantilever-based optical force sensors are difficult to apply in some specific detection fields, such as high-pressure flow detection

[a]*Tribology Research Institute, State Key Laboratory of Traction Power, Southwest Jiaotong University, Chengdu 610031, Sichuan, China. E-mail: linmao@swjtu.edu.cn*
[b]*Key Laboratory of Advanced Technologies of Materials (Ministry of Education), School of Materials Science and Engineering, Southwest Jiaotong University, Chengdu 610031, Sichuan, China. E-mail: wqyang@swjtu.edu.cn*

†Electronic supplementary information (ESI) available. See DOI: 10.1039/c7nr09076e

in environmental monitoring systems, medical instrumentation, process control, and gas pipelines.[17,18] In this regard, it is necessary to develop techniques to fabricate optical microforce sensors with both a wide detection range and a simple configuration.

In this work, we presented a high-performance optical microweighing sensor based on the synergistic effects of both a new optical projection mode and a ZnO nanorod array sensor, where a flexible T-shaped microcantilever converted applied weight into measurable photocurrent with the assistance of a UV light source. The ordered ZnO nanorod arrays, prepared by a simple low temperature hydrothermal method on an AZO glass substrate, served as the photosensitive layer. Due to its ultrahigh surface-to-volume ratio, the ZnO nanorod array structure can efficiently feed back projected area changes of the microcantilever, which is beneficial for microweighing applications. With a device size of 25 × 20 × 13 mm, the sensor can be used to measure weight based on the linearly proportional relationship between the weight and the photocurrent output, where the detection range and sensitivity are high, up to 80° and 90 nA deg^{-1}, respectively. This work presents solid progress toward the practical applications of optical microweighing in air quality monitoring and chemical and biological detection.

Design of the microweighing sensor

Fig. 1a and b show a schematic illustration and an optical image of the optical projection controllable microweighing sensor. ZnO nanorod arrays (Fig. 1c) are employed as a UV light-sensitive material in this work due to their unique optoelectronic properties, low-cost manufacturing, availability, wide range of preparation methods, and high chemical stability.[19,20] When UV light illuminates the ZnO photosensitive layer through the microcantilever, the microcantilever blocks some of the UV light and projects a projected area on the ZnO nanorod array layer. The magnitude of this projected area varies with the weight applied on the microcantilever surface. Furthermore, the magnitude of the weight can affect the deflection angle (θ) of the microcantilever, which will lead to width ($|AB|$) changes of the projected area. As shown in Fig. 1d, the width of the projected area decreases with the increment of weight from stage I to stage III. Thus, through detecting the photocurrent changes of the ZnO photosensitive layer, the magnitude of the weight can be easily measured. Importantly, the effective deflecting detection range is from 0° to 90° in theory, which is superior to that of conventional optical microweighing sensors. Therefore, if the microcantilever were functionalized with a specific molecular

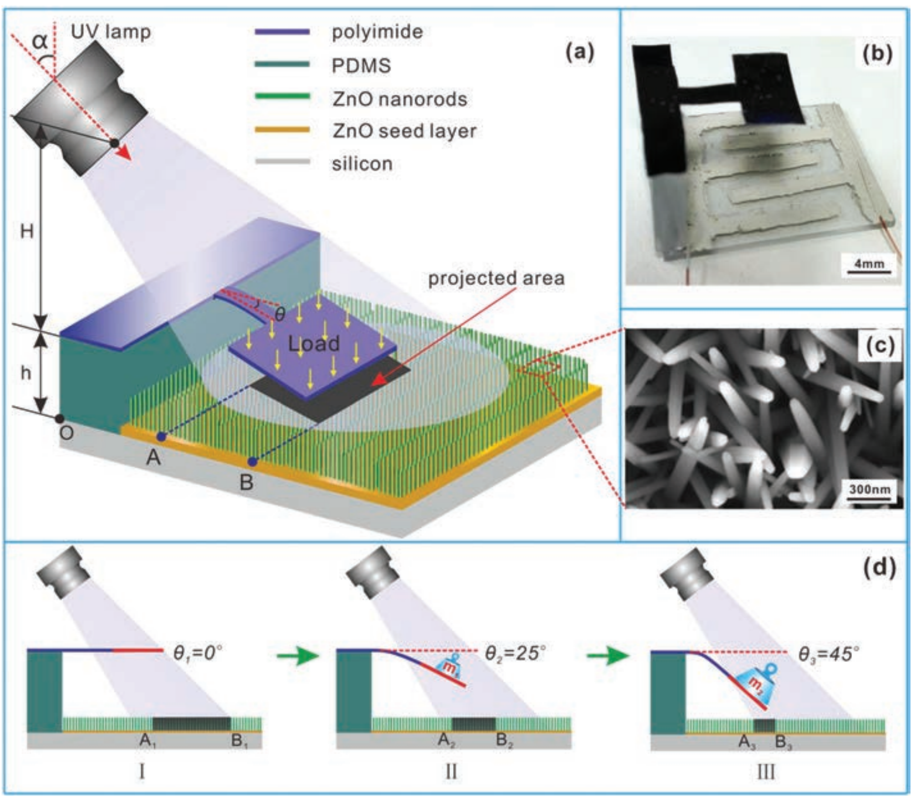

Fig. 1 Configuration design and principle of an optical microweighing sensor. (a) Schematic illustration of this optical microweighing sensor. (b) Optical image of the as-fabricated microweighing sensor. (c) Typical SEM image of the ZnO nanorod arrays. (d) Width changes (A_1B_1, A_2B_2 and A_3B_3) of the projected area under different weights.

target, this configuration could be used in chemical and biological detection fields, such as in gas sensors and virus detection.

Fabrication and characterization

Materials and fabrication of the microweighing sensor

Fig. 2 shows a schematic illustration of the fabrication process of the optical projection controllable microweighing sensor. Firstly, after cleaning in ethyl alcohol, acetone, and deionized water for 10 min in sequence, an AZO glass substrate was coated with high temperature glue, as shown in Fig. 2a. Prior to growing the ZnO nanorod arrays on the glass substrate, a ZnO seed solution (0.22 g of zinc nitrate hydrate in 5 mL of methanol) was spin-coated onto the glass substrate at 2000 rpm for 20 s, followed by sintering at 350 °C for 1 h to obtain the ZnO seed layer (Fig. 2b).[21] Then, this substrate was immersed in an aqueous solution of 0.025 M zinc nitrate hydrate (AR, Sinopharm Chemical Reagent Co., Ltd) and 0.025 M methenamine (AR, Sinopharm Chemical Reagent Co., Ltd) and heated at 90 °C for 4 h.[22–24] After this treatment, ZnO nanorod arrays were prepared on the glass substrate (Fig. 2c). To improve the collection efficiency of charge carriers,[25,26] interdigitated electrodes with a respective finger length and width of 10 and 2 mm were coated onto the ZnO photosensitive layer, as shown in Fig. 2d. The supported structure was fabricated with PDMS, which was mixed with a curing agent (Sylgard 184, Dow Corning) at a weight ratio of 10 : 1 and degassed to remove air bubbles, and then cured at 90 °C for 3 h in an oven (Fig. 2e). The microcantilever structure was fabricated with a polyimide film (thickness: 25 μm, Kapton, 100 CR) (Fig. 2f). Finally, after exposure in a UV/ozone system (PSDP UV-8T, Novascan) for 10 min, the supported structure and the microcantilever were bonded to each other on the glass substrate to form an optical microweighing sensor. Here, given the operating conditions and actual applications, the microcantilever should offer three essential properties. Firstly, the microcantilever must have excellent elasticity, which is beneficial to its repeatability, stability, and bending deformation capacity. Then, due to the high energy and destructiveness of ultraviolet light, the microcantilever should have exceptional high radiation resistance and heat resistance. Finally, tailorability and low cost are also needed, which may simplify the fabrication process and reduce production costs. Based on the above demands, polyimide is an optimal microcantilever material when compared with other polymer and inorganic materials.[27]

Structural and surface morphological characterization of the ZnO photosensitive layer

Typical scanning electron microscope (SEM) images of the ZnO seed layer (diameter, ~100 nm) and large-scale ZnO nanorod arrays are shown in Fig. 3a and b. Dense arrays of ZnO nanorods with high surface areas can be grown on glass substrates using the mild solution process described in this study. Also, the cross-sectional SEM views of the arrays (inset of Fig. 3b) suggested that the ZnO nanowires grow nearly vertically and are desirable for optical and electronic applications. Furthermore, the XRD spectrum of the ZnO photosensitive layer is shown in Fig. 3c. All the diffraction peaks of the ZnO photosensitive layer (blue line) are consistent with the values in the standard card of single-phase ZnO with a hexagonal wurtzite structure (JCPDF card no. 36-1451). No additional diffraction peaks other than ZnO were detectable, implying the high purity of the sample. Finally, high-magnification SEM imaging of the ZnO nanorod arrays reveals that the average size of the nanowires is about 100 nm wide and 6 μm long for a 4 h growth experiment, as shown in Fig. 3d.

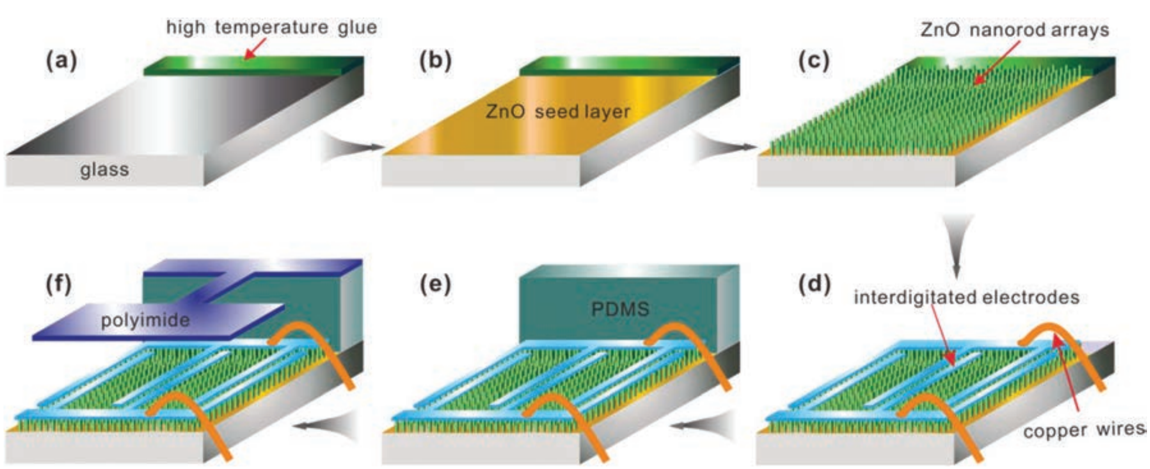

Fig. 2 Fabrication process of the optical microweighing sensors. (a) Adhering high temperature glue to the AZO glass substrate. (b) Preparing the ZnO seed layer. (c) Preparing ZnO nanorod arrays on the seed layer. (d) Fabricating interdigitated electrodes and copper wires. (e) Bonding the polydimethylsiloxane (PDMS) supported structure. (f) Bonding the polyimide microcantilever.

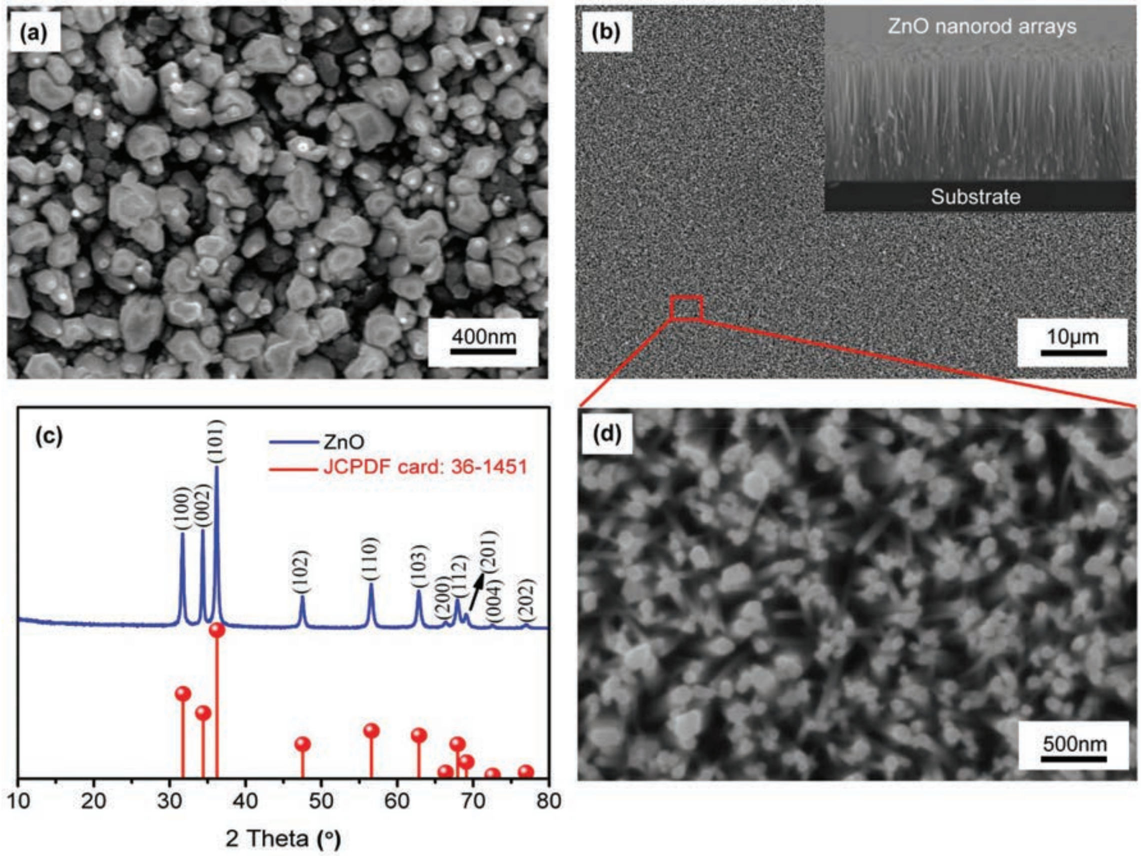

Fig. 3 Structural and surface morphological characterization of the ZnO photosensitive layer. (a) SEM image of the ZnO seed layer. (b) SEM image of the ZnO nanorod arrays. (c) X-ray diffraction (XRD) spectrum of the ZnO nanorod arrays on a glass substrate. (d) An enlarged view of the ZnO nanorod arrays.

Results and discussion

Photoelectric properties of the ZnO nanorod arrays

The electrical properties of the ZnO photosensitive layer of the optical microweighing sensor were characterized using a semiconductor parameter analyzer (Agilent B1500A, America) at room temperature. The photoresponse of the ZnO nanorod arrays was examined using a portable UV light source with an emission wavelength of 365 nm under an optical power density of 0.5 mW cm^{-2}. Fig. 4a shows the correlation between the photocurrent and UV illumination area of the microweighing sensor when a UV light source vertically irradiates the ZnO photosensitive layer. Such a linear relationship indicates that the magnitude of the output photocurrent of the as-fabricated microweighing sensor can be effectively controlled by the illumination area or shaded area, which further confirmed the feasibility of the proposed sensing principle and configuration design. Moreover, the dark current and photocurrent of the ZnO photosensitive layer are shown in Fig. 4b. Both curves are nearly linear, which suggests good Ohmic contact between the conductive silver adhesive electrode and the ZnO nanorod arrays. With 5 V applied bias, the dark current and photocurrent of the ZnO photosensitive layer are, respectively, 3.2×10^{-6} and 1.57×10^{-5} A at room temperature in ambient atmosphere, which means the ZnO layer can be applied as an effective photosensitive layer for these microweighing sensors. Finally, we also verified the correlation between illumination intensity and output photocurrent by changing the height of the UV light source. The output photocurrent obviously decreases from 15.3 μA to 8.5 μA when the height of the UV light source increases from 10 to 60 mm. Such performance degradation may have an influence on the sensitivity of the as-fabricated microweighing sensor.

Sensitivity of the microweighing sensor

Sensitivity is one of the most important parameters of sensors. For this optical microweighing sensor, the sensitivity is highly dependent on the height (H) and incident angle (α) of the UV light source. The sensitivity, k_{MCPA}, is calculated as:[28]

$$k_{MCPA} = \frac{I_{max} - I_{initial}}{90^\circ} \tag{1}$$

where $I_{initial}$ is the output photocurrent when no external weight is applied on the microcantilever, and I_{max} is the output photocurrent when the deflection angle of the microcantilever reaches its limitation (90°). Based on eqn (1), the

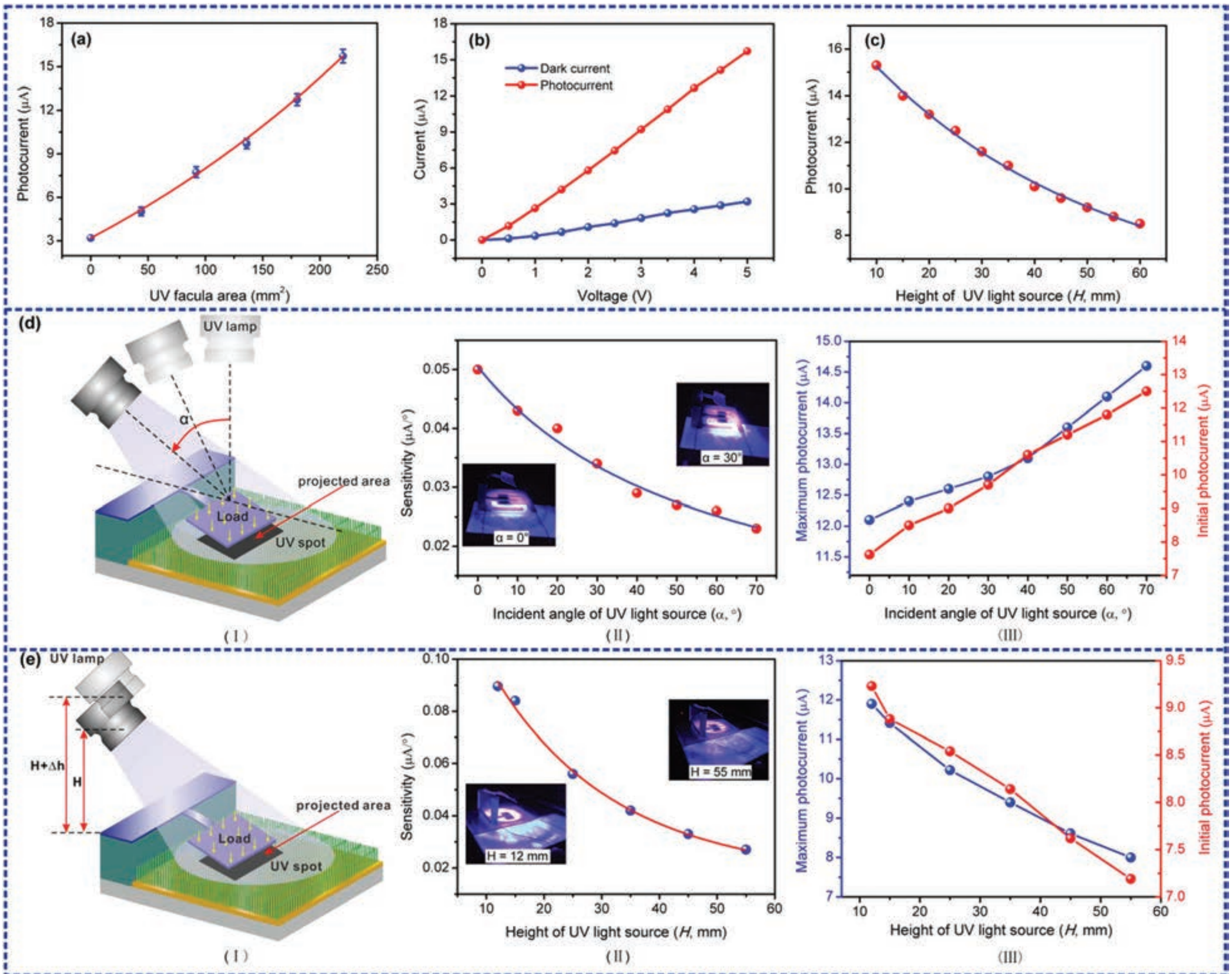

Fig. 4 Effect of *H* and *α* on the sensitivity of optical microweighing sensors. (a) Correlation between the photocurrent and UV illumination area. (b) Current to voltage (*I*–*V*) plot of the ZnO nanorods showing the dark current and photocurrent under UV light of 365 nm. (c) Correlation between the photocurrent and height of the UV light source. (d): (I) Schematic illustration of *α* adjustment. (II) Correlation between the sensitivity and incident angle. (III) The maximum and initial photocurrent under different incident angles. (e): (I) Schematic illustration of *H* adjustment. (II) Correlation between the sensitivity and height of the UV light source. (III) The maximum and initial photocurrent under different heights of the UV light source.

effect of α and H on sensitivity was investigated in order to optimize the optical microweighing sensor, and the schematic diagrams of α and H adjustment are shown in Fig. 4d(I) and e(I).

Fig. 4d(II) shows the correlation between the sensitivity and the incident angle of the UV light source. The sensitivity of the as-fabricated microweighing sensor obviously decreases from 0.05 to 0.023 μA deg^{-1} when the incident angle increases from 0° to 70°. According to eqn (1), I_{initial} and I_{max} can be affected by the incident angle of the UV light source. Hence, we further investigated the influence of the incident angle on the I_{initial} and I_{max} of the as-fabricated microweighing sensor, as shown in Fig. 4d(III). It shows that they both increase with the incident angle of the UV light source, which can be attributed to the increase of the irradiation area. Although the long axis of the UV light spot can gradually increase with the incident angle, the initial photocurrent increases faster than the maximum photocurrent, which is the key factor in sensitivity degeneration. Besides this, the projected area of the microcantilever also decreases with incident angle, which further contributes to the increase of initial photocurrent, except for the irradiation area increment (the inset of Fig. 4d(II)). Therefore, the sensitivity of this optical microweighing sensor is inversely proportional to the incident angle of the UV light source, and a highly sensitive microweighing sensor can be obtained by decreasing the incident angle.

The sensitivity can be further optimized by adjusting the height of the UV light source, as shown in Fig. 4e(II). With an increase in H from 12 to 55 mm, the sensitivity of the as-fabricated optical microweighing sensor gradually decreases from 0.09 to 0.03 μA deg^{-1}. The sensitivity deterioration with the increase in H can be attributed to a decrease in UV illumination intensity. As shown in the inset of Fig. 4e(II), the UV illumination intensity is obviously different when the height of

UV light source is 12 and 55 mm. The sensitivity deterioration can be further explained by the changes in $I_{initial}$ and I_{max}. As shown in Fig. 4e(III), $I_{initial}$ and I_{max} under different heights of the UV light source can be limited by the UV illumination intensity, but I_{max} shows double the decrement of $I_{initial}$. This is because the height changes of the UV light source did not influence the projected area of the microcantilever (the inset of Fig. 4e(II)). The output photocurrent of the projected area cannot be affected by the height changes of the UV light source, which is different from the incident angle changes. Hence, the sensitivity is inversely proportional to the height of the UV light source, and a low height of the UV light source is beneficial in improving the sensitivity of this optical microweighing sensor.

Detection range and performance of the microweighing sensor

To investigate the detection range of the optical microweighing sensor, the correlation between deflection and applied weight was calculated with a numerical simulation (ABEQUS). Table 1 shows the corresponding parameters of the numerical simulation process. Results indicated that the required external applied weights are 0, 3.3, 6.4, 10.1, 15.3, 22.5, 31.2, 41.7, and 51.6 mN when the deflection angles of the microcantilever changed from 0° to 80°. Moreover, a series of experiments were performed to further verify the accuracy of the simulation results. During the experiments, the weight applied on the microcantilever was precisely controlled by a multi-probe micro-fabrication apparatus,[29] and the deflection displacement of the microcantilever was measured by a laser displacement sensor, as shown in Fig. 5a. The actual experimental results are slightly larger than the simulation results, but they all show a good, nearly linear relationship between the deflection angles and weights, as shown in Fig. 5b. Such a nearly linear relationship is beneficial for the uniform changes of the projected area when the microcantilever undergoes a downward deflection under different external applied weights.

The microweighing performance of the as-fabricated optical microweighing sensor was further investigated based on the

Table 1 Physical properties and structure parameters of the microcantilever (Kapton film)

Thickness	Tensile modulus	Poisson's ratio	Density	b	L_1	L_2	w
25 μm	2.5 GPa	0.34	1.42 g cm^{-3}	10 mm	6 mm	6 mm	4 mm

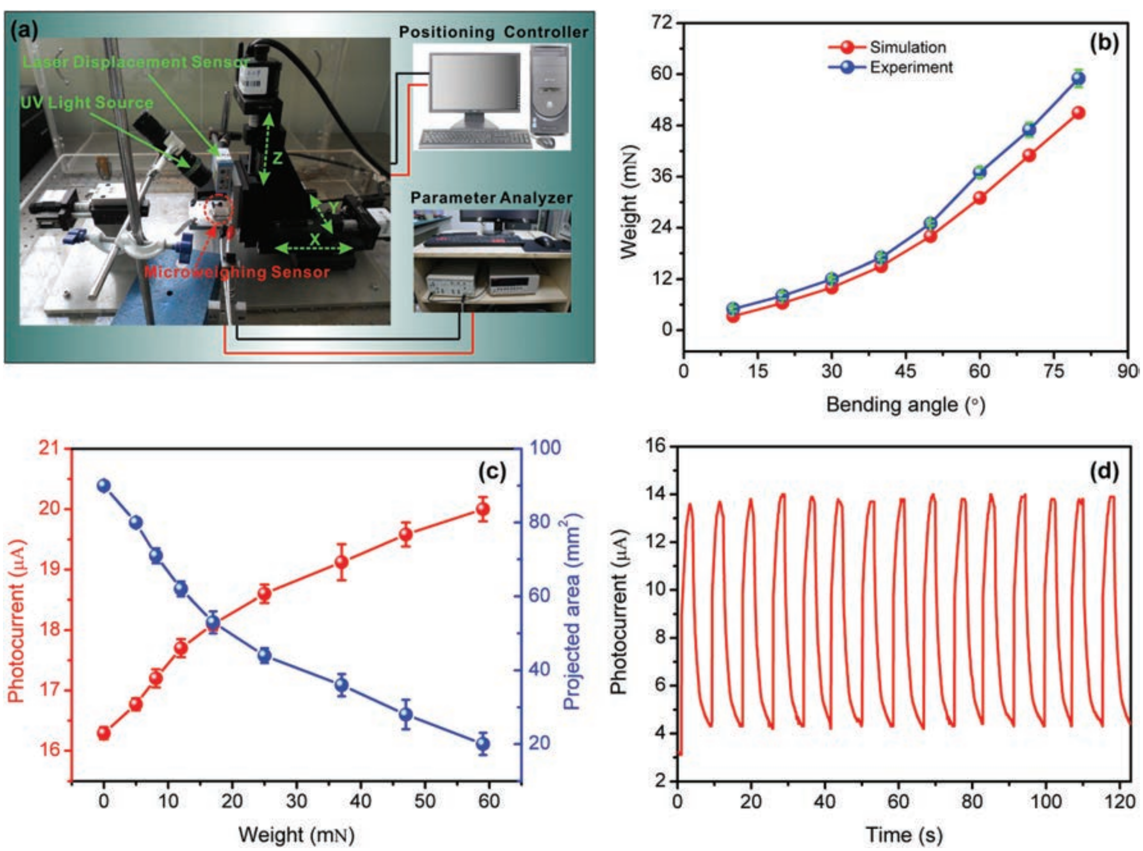

Fig. 5 Performance of the optical microweighing sensor. (a) Testing apparatus. (b) Correlation between the deflection angle and weight. (c) The output photocurrent and projected area under different applied weights. (d) Time dependence of the output photocurrent.

above experimental results. As shown by the red line of Fig. 5c, the output photocurrent increases linearly from 16.3 to 20 μA when the external weight changes from 0 to 60 mN on the microcantilever. At the same time, the projected area changes were also recorded during the testing process. It indicated that the projected area of the microcantilever decreases with an increase in external applied weight, as shown by the blue line of Fig. 5c. Such a decrement can significantly increase the output photocurrent of the ZnO photosensitive layer. Therefore, this optical projection controllable microweighing sensor can accurately detect the external weight changes. Furthermore, the time dependence of the output photocurrent of the as-fabricated sensor was also investigated, as shown in Fig. 5d. The rise and decay time constants of this optical microweighing sensor can be calculated to be about 2.5 s and 4.2 s, respectively. Note that if we utilized conventional electrodes, these photoresponse properties would be degraded significantly to 3.8 s and 4.4 s, respectively. Thus, the interdigital electrodes can effectively improve the collection efficiency of charge carriers and guarantee the repeatability and stability of the sensor.[25,30]

Effective adjustable range of the UV light source

Another advantage of this novel optical microweighing sensor is that the location of the UV spot can be adjusted within a wide range. Such a feature implies that the sensor does not need repetitive optical calibration before and after tests. A schematic illustration of the adjustment of the UV light source is shown in Fig. S3 of ESI.† The adjustable range Δx and Δy of the UV spot can be estimated as follows:

$$\Delta x = \left(\sqrt{{D_x}^2 - {L_2}^2} - b\right)/2 \tag{2}$$

$$\Delta y = \left[\frac{D_y}{\cos(\alpha - \theta_{\mathrm{uv}})} - L_2 - \left(D_y - \sqrt{{D_y}^2 - b^2}\right)\right]/2 \tag{3}$$

In this study, α and θ_{uv} are the incident angle and divergence angle of the UV light source; b and L_2 are the width (10 mm) and length (6 mm) of the guide structure; and D_x and D_y are the UV spot minor axis and major axis on the horizontal plane of the microcantilever, which can be calculated using Gaussian theory,[31]

$$D_x = 2\omega_0\sqrt{1 + \left(\frac{\lambda z}{\pi {\omega_0}^2}\right)^2} \tag{4}$$

$$D_y = 2\omega_0\sqrt{1 + \left[\frac{\lambda(z - 1/2D_x \tan\alpha)}{\pi{\omega_0}^2}\right]^2} / \sin(\alpha - \theta_{\mathrm{uv}}) \tag{5}$$

Table 3 Typical performance of some optical force sensors

Type	Effective adjustable range	Deflection range	Typical application
Optical lever[13,35,36]	Micrometer scale	<15°	AFM
Optical waveguide[15,32]	Micrometer scale	<5°	Biosensors
Photo-thermal[5]	Micrometer scale	<5°	Infrared detectors
Optical projection	>Millimeter scale	0°–80°	Air flow sensor

where w_0 and λ are the diameter (11 mm) and wavelength (365 nm), and z is the distance between the UV light source and the microcantilever (10 mm).

According to eqn (2) and (3), Δx decreases with an increase in L_2 and b for a given UV light source, and Δy can also be affected by the incident angle of the UV light source, besides L_2 and b. More about the theoretical derivation is shown in the ESI.† Therefore, Δx and Δy can be calculated with the above equations. As shown in Table 2, Δx is ±5.8 mm, and Δy increases from ±6.94 to ±8.14 mm with the increase of the incident angle from 0° to 80°. These values are much larger than those of conventional optical force sensors (usually micrometer-size).[5,13,32]

Table 3 shows a comparison of the performance of the presented optical microweighing sensor with other typical optical force sensors. The presented optical projection controllable microweighing sensor not only has a larger effective adjustable range of the location of the UV spot, but also has a larger detection range. Even though its resolution is unsatisfactory at the moment, it can be further improved by enhancing the photoelectric properties of the ZnO photosensitive layer (such as *via* intentional doping), adopting low contact resistance metallization,[33,34] and increasing the density of interdigitated electrodes. Besides this, the presented microweighing sensor is cheaper and easier to integrate into large-scale applications than conventional optical force sensors. It also can be applied in some specific areas due to its large sensing range.

Conclusions

In summary, we have demonstrated a high-performance optical microweighing sensor based on the synergistic effects of both a new optical projection mode and a ZnO nanorod array sensor. The dense ZnO nanorod arrays with high surface areas grew nearly vertically on AZO glass substrates, and the photocurrent output exhibited a good linear relationship with the projected area of the microcantilever. Ascribed to this unique configur-

Table 2 Adjustable range of the UV light source under different incident angles

α	0°	10°	20°	30°	40°	50°	60°	70°	80°
Δx (mm)	±5.80	±5.80	±5.80	±5.80	±5.80	±5.80	±5.80	±5.80	±5.80
Δy (mm)	±6.94	±6.96	±7.00	±7.09	±7.22	±7.38	±7.89	±7.84	±8.14

ation design of a sensing method, this optical microweighing sensor exhibited good linearity, a wide detection range (more than 80°), and a high sensitivity of 90 nA deg^{-1} during experiment, which is much larger than that of conventional microcantilever-based optical microweighing sensors. Furthermore, the relationship between the sensitivity and height/incident angle of the UV light source was systematically investigated in order to optimize the performance of the optical microweighing sensor. Results indicated that a low height and small incident angle of the UV light source are beneficial in obtaining highly sensitive microweighing properties. Moreover, the location of the UV light source can be adjusted within a wider range than conventional optical force sensors, which can avoid the need for repetitive optical calibration. With a wide detection range and high sensitivity, the proposed optical projection controllable microweighing sensor has potential applications in air quality monitoring and chemical and biological detection fields.

Conflicts of interest

There are no conflicts of interest to declare.

Acknowledgements

The authors are grateful for the financial support from the Natural Science Foundation of China (51527901), the Science Challenge Program of China (no. TZ2018006), and Self-developed Project of State Key Laboratory of Traction Power (2017TPL_Z02).

Notes and references

1 Y. Wei and Q. Xu, *Sens. Actuators, A*, 2015, **234**, 359–374.
2 Q. Liang, D. Zhang, G. Coppola and Y. Wang, *IEEE Sens. J.*, 2014, **14**, 2643–2657.
3 L. Hu, J. Yan, M. Liao, H. Xiang, X. Gong, L. Zhang and X. Fang, *Adv. Mater.*, 2012, **24**, 2305–2309.
4 K. Liu, C. Cheng, Z. Cheng, K. Wang, R. Ramesh and J. Wu, *Nano Lett.*, 2012, **12**, 6302–6308.
5 S. Singamaneni, M. C. LeMieux, H. P. Lang, C. Gerber, Y. Lam, S. Zauscher, P. G. Datskos, N. V. Lavrik, H. Jiang, R. R. Naik, T. J. Bunning and V. V. Tsukruk, *Adv. Mater.*, 2008, **20**, 653–680.
6 C. Grogan, L. Florea, S. Koprivica, S. Scarmagnani, L. O'Neill, F. Lyng, F. Pedreschi, F. Benito-Lopez and R. Raiteri, *Sens. Actuators, B*, 2016, **237**, 479–486.
7 R. Cabrera, E. Merced, N. Sepúlveda and F. l. E. Fernández, *J. Appl. Phys.*, 2011, **110**, 094510.
8 C. Canetta and A. Narayanaswamy, *Appl. Phys. Lett.*, 2013, **102**, 103112.
9 N. P. Siwak, X. Z. Fan, S. Kanakaraju, C. J. K. Richardson and R. Ghodssi, *Appl. Phys. Lett.*, 2014, **105**, 143102.
10 G. Putrino, A. Keating, M. Martyniuk, L. Faraone and J. Dell, *J. Lightwave Technol.*, 2012, **30**, 1863–1868.
11 S. Pham, L. Kauppinen, M. Dijkstra, H. V. Wolferen and R. D. Ridder, *IEEE Photonics Technol. Lett.*, 2011, **23**, 215–217.
12 V. T. K. Sauer, Z. Diao, M. R. Freeman and W. K. Hiebert, *Appl. Phys. Lett.*, 2012, **100**, 261102.
13 Y. Liu and J. Yang, *Nanotechnology*, 2008, **19**, 235501.
14 S.-H. T. Gajendra Shekhawat and V. P. Dravid, *Science*, 2006, **311**, 1592–1595.
15 K. Zinoviev, C. Dominguez, J. A. Plaza and L. M. Lechuga, *Appl. Phys. Lett.*, 2008, **92**, 011908.
16 T. H. Stievater, W. S. Rabinovich, M. S. Ferraro, N. A. Papanicolaou, J. B. Boos, R. A. McGill, J. L. Stepnowski and E. J. Houser, *Appl. Phys. Lett.*, 2006, **89**, 091125.
17 Y.-H. Wang, C.-P. Chen, C.-M. Chang, C.-P. Lin, C.-H. Lin, L.-M. Fu and C.-Y. Lee, *Microfluid. Nanofluid.*, 2009, **6**, 333–346.
18 Y. Wang, L. Chia-Yen and C. Che-Ming, *Sensors*, 2007, **7**, 2389–2401.
19 J. C. Fan, K. M. Sreekanth, Z. Xie, S. L. Chang and K. V. Rao, *Prog. Mater. Sci.*, 2013, **58**, 874–985.
20 J. Xu, Z. Chen, J. A. Zapien, C. S. Lee and W. Zhang, *Adv. Mater.*, 2014, **26**, 5337–5367.
21 S. Kim, J. H. Koh, X. Yang, W. S. Chi, C. Park, J. W. Leem, B. Kim, S. Seo, Y. Kim, J. S. Yu, J. H. Kim and E. Kim, *Adv. Energy Mater.*, 2014, **4**, 1301338.
22 L. E. Greene, M. Law, J. Goldberger, F. Kim, J. C. Johnson, Y. Zhang, R. J. Saykally and P. Yang, *Angew. Chem., Int. Ed.*, 2003, **115**, 3139–3142.
23 W. Deng, L. Jin, B. Zhang, Y. Chen, L. Mao, H. Zhang and W. Yang, *Nanoscale*, 2016, **8**, 1650–1656.
24 W. Deng, B. Zhang, L. Jin, Y. Chen, W. Chu, H. Zhang, M. Zhu and W. Yang, *Nanotechnology*, 2017, **28**, 135401.
25 M. Rahimi and S. R. Mikkelsen, *Anal. Chem.*, 2011, **83**, 7555–7559.
26 Ö. Ümit, D. Hofstetter and H. Morkoc, *Proc. IEEE*, 2010, **98**, 1255–1268.
27 D.-J. Liaw, K.-L. Wang, Y.-C. Huang, K.-R. Lee, J.-Y. Lai and C.-S. Ha, *Prog. Polym. Sci.*, 2012, **37**, 907–974.
28 S.-F. Wang, M.-H. Chiu, C.-W. Lai and R.-S. Chang, *Appl. Opt.*, 2006, **45**, 6702–6707.
29 Z. Wu, C. Song, J. Guo, B. Yu and L. Qian, *Front. Mech. Eng.*, 2013, **8**, 333–339.
30 E. O. Barnes, G. E. Lewis, S. E. Dale, F. Marken and R. G. Compton, *Analyst*, 2012, **137**, 1068–1081.
31 P. Goldsmith, *IEEE Press*, 1998, **5**, 192.
32 K. Okamoto, *Optics & Photonics for Counterterrorism & Crime Fighting*, 2006, vol. 7486, pp. 535–554.
33 S. J. Pearton, D. P. Norton, K. Ip, Y. W. Heo and T. Steiner, *J. Vac. Sci. Technol., B: Microelectron. Nanometer Struct. – Process., Meas., Phenom.*, 2004, **22**, 932.
34 U. Özgür, Y. I. Alivov, C. Liu, A. Teke, M. A. Reshchikov, S. Doğan, V. Avrutin, S. J. Cho and H. Morkoç, *J. Appl. Phys.*, 2005, **98**, 041301.
35 N. P. D'Costa and J. H. Hoh, *Rev. Sci. Instrum.*, 1995, **66**, 5096.
36 J. Hutter and J. Bechhoefer, *Rev. Sci. Instrum.*, 1993, **64**, 1868–1873.